Soft Matter

Mechanical Analysis of Rat Trabecular Meshwork

Journal:	*Soft Matter*
Manuscript ID:	SM-ART-08-2014-001949.R4
Article Type:	Paper
Date Submitted by the Author:	14-Jan-2015
Complete List of Authors:	Huang, Jianyong; Duke University, Biomedical Engineering Camras, Lucinda; Duke University, Biomedical Engineering Yuan, Fan; Duke University, Biomedical Engineering

Mechanical Analysis of Rat Trabecular Meshwork

Jianyong Huang[#], Lucinda J. Camras[#], and Fan Yuan[*]

Department of Biomedical Engineering, Duke University, Durham, NC 27708

[#] The first two authors contribute equally to the study.

Running title: Stiffness of Rat Trabecular Meshwork

Keywords: Trabecular Meshwork, Young's modulus, atomic force microscopy, mechanobiology, glaucoma

[*] Corresponding author:

Fan Yuan, Ph.D.
Department of Biomedical Engineering
136 Hudson Hall
Duke University
Durham, NC 27708
Phone: (919) 660-5411
Fax: (919) 684-4488
Email: fyuan@duke.edu

Abstract

Stiffness of trabecular meshwork (TM) may play an important role in regulating outflow resistance in healthy and glaucomatous eyes. However, the current techniques for stiffness measurement can only be applied to TM dissected from human donor or large animal eyes. It is a challenge to measure TM stiffness in mouse/rat eyes because of their smaller sizes and the delicate nature of TM dissection. To this end, a new technique was developed to determine the stiffness of rat TM using atomic force microscopy (AFM). In the study, rat eyes were enucleated immediately after death and perfused with a tracer (Evans blue) for 40 min. Then, the anterior segment was dissected and flat-mounted on a petri dish with TM facing upwards. An AFM probe with a gold-coated colloid tip was used to sequentially indent the corneal, TM, and uveoscleral tissues. Assuming these tissues to be neo-Hookean materials, the indentation data were analyzed with a newly developed mathematical model to calculate the apparent initial Young's moduli $(E_0)_{app}$. The geometric mean & SE of $(E_0)_{app}$ were 162 Pa & 1.2 (n = 13) for TM and 6,189 Pa & 1.4 (n = 11) for cornea; and the difference was statistically significant ($p < 0.01$). The technique established in this study allows the use of rat eye as a potential model for investigation of TM stiffness and its influences on outflow resistance. Future studies may also utilize this technique to evaluate mechanisms of TM stiffness change caused by aging, outflow dysfunction, pathogenesis of glaucoma, and drug treatment.

Introduction

Elevated intraocular pressure (IOP) is the key risk factor for development of primary open-angle glaucoma (POAG), due to increased resistance to aqueous humor outflow that occurs predominantly at the juxtacanalicular tissue (JCT) of the trabecular meshwork (TM) and the inner wall of Schlemm's canal (SC).[1, 2] The resistance increase is correlated to changes in TM stiffness that can influence the extent of deformation of TM and inner wall of SC. It has been shown that JCT expansion and pore formation in the endothelium of SC reduce outflow resistance.[3-8] Additionally, the outflow resistance may be affected by radial movement of TM in response to pulsation and non-periodic fluctuations of IOP,[5, 9, 10] if the movement causes occlusion of SC or closing of collector channels. The dependence of outflow resistance on TM stiffness has led to the development of a new class of anti-glaucoma drugs (e.g., rho kinase inhibitors) that decrease the outflow resistance by relaxing TM cells.[2, 11]

Stiffness of TM has been evaluated in glaucomatous and normal human eyes at local (or microscopic) and tissue levels.[12-14] The local stiffness of JCT and inner wall of SC, measured with atomic force microscopy (AFM), was observed to be stiffer in glaucomatous than non-glaucomatous TM,[12] although the local stiffness has yet to be correlated directly to changes in outflow function. The correlation analysis has been performed only for normal porcine eyes, which showed that it was statistically insignificant.[15] At the tissue level, the circumferential tensile Young's modulus of the human TM has been measured through a uniaxial stretching test. The data showed that a stiffer TM was correlated with a lower outflow resistance in non-glaucomatous eyes.[13] This correlation was not observed in glaucomatous eyes.[14] Another key observation in the human TM studies was that the non-glaucomatous TM was four times as stiff as the glaucomatous TM, which was opposite to the observation of local stiffness of the JCT and inner wall of SC.[12] The apparent discrepancy suggests that pathological changes in the eyes caused by glaucoma lead to a reduction in the tensile stiffness of TM, which depends mainly on the uveal and corneoscleral meshworks, but an increase in compressive stiffness of JCT and inner wall of SC.[14]

Mechanisms behind the relationship between outflow function and TM stiffness are complicated, and require more quantitative investigation. However, a challenge for the investigation is that human donor eyes provide few opportunities for evaluation of *in vivo* mechanisms that could affect TM stiffness and outflow function, prior to the mechanical testing *ex vivo*. To solve this problem and understand mechanisms of outflow regulation *in vivo*, it is critical to develop animal models for tissue stiffness analysis.

Rats and mice have been used ubiquitously in ophthalmology research due to their availability, low cost, and similarities in ocular tissue structures to humans. Specifically, similarities have been observed in conventional aqueous outflow pathways that are characterized with continuous TM and SC.[16-19] Furthermore, various methods have been established for determining outflow function in rats[20] and mice.[21-24] However, there have been no reported attempts at measuring TM stiffness, presumably due to the inherent difficulty in handling mouse and rat TMs. Unlike human and porcine TMs,[13, 14] they are too small to be manually isolated without damaging and pre-stretching the tissue. Therefore, we developed a method to evaluate rat TM stiffness *in situ*. The method was based on a technique for flat mounting rat anterior segments developed previously to visualize TM,[25, 26] and the AFM, which can accommodate the smaller size of rat eyes, for tissue stiffness measurements. The approximate location of TM was identified microscopically with the use of Evans blue dye that preferentially accumulated in TM after prolonged intracameral infusion. The AFM data was analyzed with a new mathematical model developed in this study to obtain the distribution profile of the initial Young's modulus of tissues across the Evans blue stained region. We also performed numerical simulations of nonlinear indentation of soft tissues to validate the new method.

Experimental

Eye tissue preparation

For better differentiation of iris, ciliary muscle, and choroid in ocular tissue dissection, pigmented rather than albino rats were used for TM stiffness evaluation (Long-Evans rats, Charles River Labs International Inc., Raleigh, NC). After the rats were sacrificed, the superior

regions of the left (i.e., OS) and right (i.e., OD) eyes were marked *in situ* before they were enucleated. For the *ex vivo* perfusion of whole eyes, a microneedle connected to a solution reservoir filled with a tracer (Evans blue at 0.5 mg/mL) was placed in the anterior chamber (**Figure 1A**), the meniscus of the solution reservoir height was raised to approximately 20 cm above the eye, setting the perfusion pressure at 15 mmHg; and the eyes were perfused for 40 min. Extended perfusion allowed the tracer to accumulate in the outflow pathways (both unconventional and conventional) to assist the identification of TM location.

It was expected that the tracer accumulated in tissues should have minimal effects on TM stiffness because Evans blue is a small molecule dye with little known biological functions. To confirm it experimentally, we dissected the TM from a porcine eye after it was perfused *ex vivo* with the Evans blue solution, and measured its Young's modulus with AFM. The measurement was repeated at different locations on the same TM with varying blue color intensities, which were scored visually between 1 and 5. We observed no correlation between the Young's modulus and the blue color intensity ($R^2 = 0.0437$, n = 6), and the average value of the Young's modulus to be 1.03 kPa. We also measured the Young's modulus of TM from nine porcine eyes not perfused with the Evans blue solution (i.e., the control), and observed that the mean±SD and median of the data were 1.31±1.25 kPa and 0.72 kPa, respectively (n = 9). These data demonstrated that effects of Evans blue staining on TM stiffness was negligible compared to the variation in the Young's modulus within a TM or among different TM tissues.

After the perfusion, the eyes were dissected at the posterior pole, and the lens and retina were removed. Then, a small blade and a forceps were used to carefully scrap and detach the uveal tissues (choroid, ciliary body, and iris) from the anterior segment. To avoid damage of the Evans blue-stained tissues, portions of ciliary body and iris near the scleral spur remained intact, which could be observed in the histological examination (see the Results section). The incomplete dissection was in fact advantageous for differentiation between the blue dye stained TM and the pigmented uveal tissues. The dissected anterior segments were then flat-mounted with the TM facing upwards (**Figures 1B & 1C**). The Evans blue stained tissues could be

observed clearly in all samples, and were used to identify the approximate location of TM relative to the pigmented uveal tissues. Broken coverslips were used to glue down the sclera (**Figure 1D**), and secure the dissected anterior segment for AFM. The temporal and nasal positions were identified for each eye prior to AFM measurement. The tissue preparation procedures were finished within 2 hours post-mortem.

Local stiffness measurement with atomic force microscopy

Flat-mounted anterior segments were submerged in phosphate buffer solution (PBS), and placed under an AFM (MFP-3D, Asylum Research, Santa Barbara, CA). A typical image of the anterior segment taken optically under the AFM is shown in **Figure 2**. Although the color of Evans blue stained tissues was weak in some samples, the pigmented uveal tissues, which were located next to the blue tissues (see **Figures 1B and 1C**), could be observed clearly. Therefore, both the pigmented and the blue tissues were used to guide the division of the area shown in **Figure 2** into five different regions. Region 1was relatively transparent, which was identified as the cornea; and Region 5 contained the pigmented uveal residue and the scleral tissues. Together, they were called "uveosclera." The area between Region 1 and Region 5 was divided into three regions. Region 3 was most likely to be located in TM although its exact location was unknown. Regions 2 and 4 were considered to be the border regions between TM and its surrounding tissues (i.e., cornea and uveosclera). The differentiation of these regions was evaluated and confirmed at the end of the study through comparisons of both the tissue stiffness data obtained experimentally; and the differentiation was verified with the results from numerical simulations.

The AFM probe used for tissue indentation had a labeled spring constant of 0.08 N/m and a colloid tip (Novascan Technologies, Ames, IA). The tip was spherical and coated with gold; and its radius (R) was 2.5 μm. The probe was always calibrated prior to the first measurement on the experiment day to determine its actual spring constant (k_z). Prior to indentation, an area next to the pigmented area was randomly selected; and each of the five regions was indented with the AFM probe at a velocity of 5 μm/sec. Only one indentation curve per region was used to determine the tissue stiffness. During tissue indentation, the deflection of cantilever (d) and piezo-actuator translation (z) were measured experimentally. They were then used to calculate

the indentation force, F, and w, where $F = k_z(d - d_c)$, $w = z - d$, and d_c is the value of d at the contact point. In the literature, the F *vs.* w curves are often fitted with the Hertz equation,

$$F = \frac{4E_H}{3(1-\nu^2)} R^2 \beta^{\frac{3}{2}} \quad (1)$$

to determine both the value of w at the contact point (w_c) and the Hertz Young's modulus (E_H) of tissues, where ν is the Poisson's ratio, $\beta = \delta/R$, and $\delta = w - w_c$. However, the use of the Hertz equation requires tissues to be linear elastic and homogeneous, and the contact region to be non-adhesive.[27-29] Furthermore, it requires $\beta < 0.1$, i.e., tissue deformation is infinitesimal. Such a requirement could be satisfied for hard tissues/materials but impractical for soft ones, such as TM, because a large β was necessary for the cantilever deflection (d) to be measured accurately. To overcome this problem, we derived a new equation to analyze the experimental data, assuming that the ocular tissues within each region defined above were homogeneous neo-Hookean materials. Details of the derivation are described in the **Supplementary Information** section. The new equation is expressed as,

$$F = \frac{4E_0}{3(1-\nu^2)} R^2 \beta^{\frac{3}{2}} (1 + \theta\beta^{\frac{1}{2}}) \quad (2)$$

where E_0 is the initial Young's modulus of the tissue, and θ is a constant. To determine the value of θ and validate **Equation 2**, we performed numerical simulations of tissue indentation with an AFM probe (see the **Supplementary Information** section). Results of the simulation showed that **Equation** 2 could be used to accurately determine the value of E_0 for a semi-finite half space, with an error of $< 0.05\%$, if $\theta = -0.089$ (see Table S1) and $\beta \leq 0.5$.

In indentation experiments, there existed structural heterogeneity of ocular tissues and uncertainty in AFM probe locations relative to the TM. Hence, experimentally data analysis with **Equation** 2 could only yield an apparent initial Young's modulus $(E_0)_{app}$. To determine $(E_0)_{app}$, we chose the upper limits of the data to be 5.0 nN for F [28] and 0.5 for β whoever was reached first, except for a few very soft samples that had $(E_0)_{app} < 100$ Pa and $R^2 < 0.9$ in regression analysis. For these tissues, the upper limits were changed to 1.0 nN for F and 0.8 for β because the extent of indentation for very soft tissues had to be sufficiently large in order for d to be

larger than the detection limit of AFM. The lower limit of F was chosen to be one-third of its upper limit determined above, because the exact location of the contact point was unknown before the regression analysis. In regression analysis of experimental data, we also observed that the nonlinear regression analysis with **Equation 2** was unstable. Thus, we first performed a linear regression analysis with **Equation 1** to determine the location of the contact point, and then used it to determine the value of E_0 through another linear regression analysis with **Equation 2**. The quality of curve fitting is indicated with R^2. The error caused by the two-step approach to data analysis is discussed in the Discussion section.

To estimate the difference between $(E_0)_{app}$ and E_0, we developed a mathematical model and performed another set of numerical simulations to generate F *vs.* δ curves, based on a model geometry similar to ocular tissues observed in histological sections (see the **Supplementary Information** section). The numerically generated F *vs.* δ curves were analyzed to determine the simulated $(E_0)_{app}$, using the method described above for experimental data analysis, which was then compared to E_0 given in the simulation.

Histology

Histological analysis was performed for a fraction of the rat eyes to confirm the integrity of TM tissues post-dissection. To achieve it, anterior segments were immersed in 2.5% glutaraldehyde and 2% paraformaldehyde, and embedded in Spurr resin. The resin was then cut into 0.4 to 0.5 μm thin sections, and stained with 1% methylene blue.

Statistics

All data were evaluated to determine distributions using box-and-whisker plots. If a distribution was observed to be significantly asymmetric about the median, the data would be logarithmically transformed. ANOVA was performed for data measured in five different tissue regions and paired eyes, using Statview software (Abacus Concepts, Inc., Berkeley, CA). Fisher's Protected Least Significant Difference (PLSD) post hoc test was used to determine differences between two groups. A difference was considered to be statistically significant if the p-value was less than 0.05.

Results

Seven pairs of rat eyes were prepared for the study. One of the left eyes was discarded due to a cut in sclera during enucleation, which made it unsuitable for dye perfusion. The other 13 eyes were marked to indicate the nasal and temporal regions. Histological analysis confirmed the presence of the TM in the flat mounted anterior segments although partial damage to the anterior TM near the cornea might happen during tissue fixation/preparation (**Figure 3**). The presence of uveal tissues was also evident in both histological and AFM images.

For each anterior segment, the five tissue regions defined in **Figure 2** were indented sequentially with the AFM probe. A typical force versus indentation curve is shown in **Figure 4**. The experimental data were fitted with **Equation 2** to determine the apparent initial Young's modulus, $(E_0)_{app}$. The R^2-values in all regression analyses were observed to be greater than 0.9. The results of $(E_0)_{app}$ for all five regions in an eye are shown in **Figure 5**. Multiple indentations were performed in both nasal and temporal regions of the 13 eyes, and the data showed insignificant differences in $(E_0)_{app}$ between the two regions. Thus, all data from the same eye were pooled together and averaged; and the mean values of $(E_0)_{app}$ for each eye are reported in **Table 1**. It should be noted that we could not measure $(E_0)_{app}$ for all five regions in some eyes, because indentation curves from certain regions in these eyes were irregular and significantly different from predictions by any mechanical theories. Thus, they were discarded in our data analyses. This technical issue was caused presumably by problems in tissue preparations.

Box-and-Whisker plots of $(E_0)_{app}$ reported in **Table 1** are also shown in **Figure 6A**, a magnified plot of $(E_0)_{app}$ in Region 3 (or TM) is shown as the insert in the same figure, and the logarithmically transformed $(E_0)_{app}$ with base 10, $\log_{10}E$, are plotted in **Figure 6B**. A two-way ANOVA was performed to compare $\log_{10}E$ in different tissue regions from paired eyes for Animals #2 through #7. Results of the analysis indicated a significant difference in $\log_{10}E$ between different tissue regions ($p < 0.001$), but not between paired eyes ($p > 0.05$). Additionally, there were insignificant interactions between tissue region and eye location (i.e.,

left or right side) (tissue region × eye location, $p > 0.05$), demonstrating that the variation in $\log_{10}E$ with tissue region was statistically independent of the eye location. To further compare the experimental data, we chose the data of $\log_{10}E$ from the seven right eyes only, and performed a one-way ANOVA. The new analysis showed again that there was a significant difference in $\log_{10}E$ between different tissue regions ($p < 0.01$); and $\log_{10}E$ was the smallest in Region 3 and the largest in Region 1 (see **Table 2**).

$(E_0)_{app}$ determined with **Equation 2** differed from E_0, a material property of the tissue, because the former also depends on location of indentation, tissue geometry, and stiffness of surrounding tissues. To estimate the difference between the apparent and the actual initial Young's moduli, we developed a mathematical model (see the **Supplementary Information** section) to numerically simulate the AFM indentation. The model geometry is shown in **Figure S2**, and the indentation *in silico* was performed at different locations on the top surfaces of uveosclera, TM, and cornea. A typical image of the simulated distribution of the total tissue displacement is shown in **Figure 7**, which demonstrated that although tissue deformation occurred throughout the entire volume, large deformation occurred only in a small region under the AFM probe, indicating that $(E_0)_{app}$ was determined mainly by mechanical properties of cells and extracellular matrix in that small region. To quantitatively determine the difference between $(E_0)_{app}$ and E_0, we chose the values of E_0 for uveosclera, TM, and cornea to be approximately equal to the corresponding geometric means of $(E_0)_{app}$ determined experimentally (see **Table 1**), and simulated indentation force F as a function of δ/R for different experimental scenarios. The simulated profiles of F *vs.* δ/R were fitted with **Equation 2** to obtain $(E_0)_{app}$. The results shown in **Table 3** indicated that $(E_0)_{app}$ was close to E_0 if the upper limit of δ was chosen to be $0.5R$. If the indentation was performed at uveosclera and cornea, the errors were < 1.5%. If the indentation was performed at TM, the maximum error was increased to 19%. For very soft TM, we had to increase the upper limit of δ to $0.8R$ in experimental data analysis (see the Methods section). The impact of the increase in the upper limit was estimated through the numerical simulations. Results from the simulation showed that the maximum difference between $(E_0)_{app}$ and E_0 was increased from 19% to 24% if the upper limit of indentation was increased from $0.5R$ to $0.8R$, because of the nonlinear tissue deformation that was not fully considered in **Equation 2**.

As mentioned above, partial damage to the anterior TM might happen in tissue fixation/preparation (**Figure 3**), which could cause partial detachment of TM from the cornea. To quantitatively determine how the partial detachment affected TM stiffness measurement, we performed another set of simulations, using a new model geometry in which >57% of the connection between TM and cornea were removed (see **Figure S3**). Results from the simulation showed that TM detachment would reduce the influence of cornea on the fitted $(E_0)_{app}$ (see **Table 4**). As a result, only $(E_0)_{app}$ near the anterior edge of TM was decreased significantly. Overall, the simulation results suggested that the values of $(E_0)_{app}$ determined experimentally with **Equation 2** were accurate estimations of E_0 for corneal and uveoscleral tissues. For TM, the difference between $(E_0)_{app}$ and E_0 was dependent on the location of indentation, and the maximum difference was 24% for the scenarios considered in this study.

Discussion

The current study provided the first measurement of the apparent initial Young's modulus of TM in rat eyes. Among the five regions defined in a flat-mounted anterior segments (see **Figure 2**), the region that had the strongest Evans blue staining and the lowest value of $(E_0)_{app}$ (Region 3) was identified as the TM. Differences in $(E_0)_{app}$ between nasal and temporal areas, and between paired eyes were statistically insignificant for all five regions. The difference between $(E_0)_{app}$ and E_0 of TM was estimated through analysis of *in silico* indentation of anterior segment. Results from the analysis demonstrated that $(E_0)_{app}$ was a good estimate of E_0 with a maximal error being on the order of 20%.

Variation in tissue stiffness

Tissue stiffness depends on its compositions characterized by extracellular matrix (ECM) composition (e.g., glycosaminoglycans and collagens) and density, cell type and density, and extent of tissue hydration. Stiffness of cells and ECM can differ significantly. Even within a cell, there might be 100-fold variation in the Young's modulus across different regions.[30] Therefore,

$(E_0)_{app}$ measured with AFM is location dependent. Statistically, we did not observe differences in $(E_0)_{app}$ between nasal and temporal areas within the same eyes, or between the paired eyes. Thus, we only reported the average stiffness of nasal and temporal areas, and considered data from paired eyes as repeated measurements.

Significant variation in tissue stiffness was observed among different regions defined in **Figure 2**. To determine $(E_0)_{app}$ of TM, we assumed that the TM was softer than other tissues. The assumption was also one of the two criteria for identification of TM location in the anterior segment. It was based on experimental data in previous studies,[31] which showed that the Young's modulus of TM measured with AFM[12, 15] is significantly lower than those of cornea[32] and episcleral region of sclera,[33] for both human[12, 32] and porcine[15, 33] eyes. It is unclear why TM is softer than cornea and sclera, but structurally such an observation would be expected since TM consists of a loose meshwork of tissues plus a thin layer of JCT. It is small, and sandwiched between two fluid compartments: the anterior chamber and the SC. In contrast, cornea and sclera are much larger, and contain densely packed networks of collagen fibrils.[34] As a result, cornea and sclera should be more resistant to indentation than TM.

To further understand the data measured at different regions, we performed numerical simulations of tissue indentation under the conditions chosen to be close to those observed in experiments. Results from the simulations showed that the apparent Young's moduli $(E_0)_{app}$ of tissues in Regions 2 and 4 should be close to $(E_0)_{app}$ of a tissue, either TM, corneal, or uveoscleral (see **Table 3**), rather than between the $(E_0)_{app}$ of two adjacent tissues. The prediction differed from those shown in **Table 1**; and the discrepancy could be explained by two possible scenarios. One is that there exists a gradual transition in stiffness between different tissues, which was not considered in our mathematical model. Another scenario is that some of the measurements in Regions 2 and 4 were in fact performed at TM because these regions could also be stained with Evans blue (see **Figure 5**). Additionally, the experimental data for Region 5 was not a measure of stiffness for a specific tissue since this region might contain remnants of uveal tissues (choroid, iris, and ciliary body) in addition to sclera, because it was impossible to remove all uveal tissues without damaging TM. Taken together, we could state that the experimental data

of $(E_0)_{app}$ for Regions 2, 4, and 5 did not have unique structural basis, they were the mixture of data from different tissues, and only the experimental data of $(E_0)_{app}$ for Regions 1 and 3 were tissue specific, which were reliable measurements of the mechanical properties of cornea and TM, respectively.

It is also important to point out that rat TM measured in this study was significantly softer than a cell measured in previous studies;[35, 36] and the compressive Young's modulus of cells is at least two orders of magnitude smaller than that of collagen fibrils under tensile stress.[37, 38] The low stiffness of TM is likely to be attributable to loose structures of the meshwork with its ECM fibers and collagen beams aligned approximately in the direction perpendicular to that of outflow or the direction of tissue indentation for stiffness measurement.[13] This type of tissue structures provide high resistance to stretching in the circumferential direction,[13, 14] but low resistance to tissue deformation in the outflow direction. The low stiffness may explain why TM can oscillate in response to small changes (± 3 mmHg) in IOP,[10] which has been considered to be important for regulation of outflow resistance.[5, 9]

Error analysis

Ocular tissues are non-uniform, and contain distinct multi-cellular structures. To simplify the error analysis, we assumed that the structures involved in this study consisted of only three tissues: TM, cornea, and uveosclera, and that each tissue was a homogeneous neo-Hookean material. Thus, the measured $(E_0)_{app}$ shown in **Table 1** was an average property of tissues under the AFM probe; and the measurement of $(E_0)_{app}$ was dependent on the location of indentation.

The main source of errors in determining the initial Young's modulus of TM was the assumption used in the derivation of **Equation 2**, that the indented tissue was uniform and infinitely large. The assumption neglected the bending of TM towards the outer wall of SC, caused by the indentation with an AFM probe, and the influences of uveosclera and cornea on TM indentation. To estimate the resulted errors in experimental data analysis, we performed numerical simulations. Results from the simulation showed that the maximum difference between E_0 and simulated $(E_0)_{app}$ was 24%, occurred near the center of the TM (x_0 = 72.5 μm in

Figure S2) when the upper limit of the indentation was 0.8*R*. This error was acceptable, compared to the extent of variation in the $(E_0)_{app}$ of TM (see **Table 1**).

Another source of errors was that we determined the contact point through fitting the experimental data with the Hertz equation (i.e., **Equation 1**) instead of using **Equation 2** for simultaneous determination of both the contact point and $(E_0)_{app}$. This was because the latter approach involved nonlinear curve fitting that was observed to be unstable. To estimate the error in the contact point determined in the current study, we numerically simulated ocular tissue indentation with w_c being set to zero (see **Figure 7**), fit the simulated F vs. w curves with the Hertz equation to generate a new value of w_c, which differed from zero, and then used this value of w_c to determine $(E_0)_{app}$ with **Equation 2**. It was observed that the maximum deviation of w_c from zero was 4.2% of the total indentation; and the resulted error in $(E_0)_{app}$ was less than 6.6%, compared with the value of $(E_0)_{app}$ determined with w_c being set to zero.

Conclusions

The study provided the first method to measure TM stiffness in a rat model. It showed that TM was significantly softer than other tissues in surrounding regions. Statistically, there were no significant differences in tissue stiffness between paired eyes and between nasal and temporal areas within the same eye, indicating that in future studies, if TM stiffness is altered in one eye, the contralateral eye can be used as a control. The new technique is expected to create numerous opportunities for investigators to manipulate TM stiffness *in vivo* and determine quantitatively how the stiffness change affects outflow function within the same eyes. It will also allow investigators to explore mechanisms that may lead to stiffness changes in the TM and test new drugs that target the outflow pathway.

Table 1: Apparent Initial Young's Modulus in Different Regions

		Tissue Region				
Rat	**Eye** †	**1**	**2**	**3**	**4**	**5**
1	OD		2830.6	177.9	387.9	519.8
2	OD	21281.8	3487.6	247.2	1997.8	7240.5
2	OS *	1593.7	550.4	172.1	596.1	
3	OD	19333.0	1121.9	253.9		257.7
3	OS	14674.0	5401.1	215.7	4647.5	9668.7
4	OD	7276.1	6140.8	110.8	3340.3	777.9
4	OS	8673.5	2664.9	207.2	721.3	
5	OD **	3089.6	833.2	127.8	2470.2	3412.7
5	OS *		800.9	354.8	5668.1	3862.2
6	OD **	1820.0	128.2	74.4	228.9	1354.3
6	OS **	7041.7		233.7	1210.8	
7	OD	13620.0		95.3	934.6	1843.6
7	OS	1558.4	1570.5	71.8	316.7	4563.2
Geometric Mean (Pa)		**6189.0**	**1475.9**	**161.6**	**1160.1**	**2013.5**
Geometric SE		**1.35**	**1.41**	**1.15**	**1.36**	**1.45**

† Data obtained from the nasal and temporal regions were averaged for each eye, except for those specified with asterisks: * only from the nasal region; ** only from the temporal region. OS: left eye, and OD: right eye.

Table 2: Results from Fisher's PLSD Post-hoc Test †

	1 (n=6)	**2** (n=6)	**3** (n=7)	**4** (n=6)	**5** (n=7)
1		**< 0.01**	**< 0.001**	**< 0.01**	**< 0.01**
2			**< 0.001**	> 0.05	> 0.05
3				**< 0.01**	**< 0.001**
4					> 0.05

† Differences in $\log_{10}$E of TM between different tissue regions were compared. Only the data from Regions 1 through 5 in the right (i.e., OD) eyes were used in the comparison. The table shows the p-values from the comparisons. n denotes the number of eyes in each group.

Table 3: Comparison of E_0 and $(E_0)_{app}$ Obtained from Numerically Simulated Indentation of Ocular Tissues †

x_0 (μm)	Tissue Type	E_0 (Pa)	$(E_0)_{app}$ (Pa)	Percent difference
-40	Uveosclera	2000	2021	1.1%
-17.5	Uveosclera	2000	1979	1.1%
5	TM	160	175	9.4%
27.5	TM	160	149	6.9%
50	TM	160	136	15%
72.5	TM	160	129	19%
95	TM	160	170	6.3%
117.5	Cornea	6200	6119	1.3%
140	Cornea	6200	6182	0.3%

† In the simulation, all tissues were assumed to be neo-Hookean materials with E_0 of TM, cornea, and uveosclera being fixed at 160 Pa, 6200 Pa, and 2000 Pa, respectively. The indentation force (F) was simulated as a function of δ/R, where δ is the indentation and R is the tip radius of AFM probe. The simulated F vs. δ/R curves were fitted with **Equation 2** to yield the values of apparent initial Young's modulus, $(E_0)_{app}$. Then, the percent difference between the given E_0 and the fitted $(E_0)_{app}$ was calculated.

Table 4: Effects of Partial Detachment of TM on Simulated $(E_0)_{app}$ of TM †

x_0 (μm)	$(E_0)_{app}$ (Pa)	Error for intact TM	$(E_0)_{det}$ (Pa)	Error for detached TM
5	175	9.4%	175	9.4%
27.5	149	6.9%	149	6.9%
50	136	15%	134	16%
72.5	129	19%	126	21%
95	170	6.3%	154	3.8%

† Indentation of partially detached TM was simulated numerically. The procedure of simulations was the same as that described in Table 3. The values of $(E_0)_{app}$ for intact TM are copied from Table 3 for comparisons with $(E_0)_{det}$ that denotes the value of $(E_0)_{app}$ of partially detached TM at the same horizontal locations (x_0). The error was calculated as the percent difference between E_0 and $(E_0)_{app}$ for intact TM, or between E_0 and $(E_0)_{det}$ for detached TM.

References

1. W. M. Grant, *Trans Am Acad Ophthalmol Otolaryngol*, 1951, **55**, 774-781.
2. D. R. Overby, W. D. Stamer and M. Johnson, *Experimental eye research*, 2009, **88**, 656-670.
3. E. H. Zhou, R. Krishnan, W. D. Stamer, K. M. Perkumas, K. Rajendran, J. F. Nabhan, Q. Lu, J. J. Fredberg and M. Johnson, *Journal of the Royal Society, Interface / the Royal Society*, 2012, **9**, 1144-1155.
4. G. Li, S. Farsiu, S. J. Chiu, P. Gonzalez, E. Lutjen-Drecoll, D. R. Overby and W. D. Stamer, *Investigative ophthalmology & visual science*, 2014, **55**, 3737-3746.
5. M. A. Johnstone, *Journal of ocular pharmacology and therapeutics : the official journal of the Association for Ocular Pharmacology and Therapeutics*, 2014, **30**, 88-93.
6. M. Johnson, D. Chan, A. T. Read, C. Christensen, A. Sit and C. R. Ethier, *Investigative ophthalmology & visual science*, 2002, **43**, 2950-2955.
7. C. R. Ethier, F. M. Coloma, A. J. Sit and M. Johnson, *Investigative ophthalmology & visual science*, 1998, **39**, 2041-2048.
8. M. Johnson, A. Shapiro, C. R. Ethier and R. D. Kamm, *Investigative ophthalmology & visual science*, 1992, **33**, 1670-1675.
9. R. F. Ramos and W. D. Stamer, *Investigative ophthalmology & visual science*, 2008, **49**, 275-281.
10. P. Li, R. Reif, Z. Zhi, E. Martin, T. T. Shen, M. Johnstone and R. K. Wang, *Journal of biomedical optics*, 2012, **17**, 076026.
11. C. Y. Yang, Y. Liu, Z. Lu, R. Ren and H. Gong, *Investigative ophthalmology & visual science*, 2013, **54**, 5859-5870.
12. J. A. Last, T. Pan, Y. Ding, C. M. Reilly, K. Keller, T. S. Acott, M. P. Fautsch, C. J. Murphy and P. Russell, *Investigative ophthalmology & visual science*, 2011, **52**, 2147-2152.
13. L. J. Camras, W. D. Stamer, D. Epstein, P. Gonzalez and F. Yuan, *Investigative ophthalmology & visual science*, 2012, **53**, 5242-5250.
14. L. J. Camras, W. D. Stamer, D. Epstein, P. Gonzalez and F. Yuan, *Investigative ophthalmology & visual science*, 2014, **55**, 814-823.
15. F. Yuan, L. J. Camras and P. Gonzalez, ARVO, Fort Lauderdale, FL, 2011.
16. C. Reme, U. Urner and B. Aeberhard, *Graefes Arch Clin Exp Ophthalmol*, 1983, **220**, 139-153.
17. R. C. Tripathi and B. J. Tripathi, *Experimental eye research*, 1972, **14**, 73-79.
18. J. C. Morrison, F. W. Fraunfelder, S. T. Milne and C. G. Moore, *Investigative ophthalmology & visual science*, 1995, **36**, 751-756.
19. D. R. Overby, J. Betrand, O. Y. Tektas, A. Boussommier-Calleja, M. Schicht, C. R. Ethier, D. F. Woodward, W. D. Stamer and E. Lutjen-Drecoll, *Investigative ophthalmology & visual science*, 2014, **in press**.
20. A. Mermoud, G. Baerveldt, D. S. Minckler, J. A. Prata, Jr. and N. A. Rao, *Graefes Arch Clin Exp Ophthalmol*, 1996, **234 Suppl 1**, S198-203.
21. M. Aihara, J. D. Lindsey and R. N. Weinreb, *Investigative ophthalmology & visual science*, 2003, **44**, 5168-5173.

22. Y. Zhang, B. R. Davidson, W. D. Stamer, J. K. Barton, L. Y. Marmorstein and A. D. Marmorstein, *Investigative ophthalmology & visual science*, 2009, **50**, 765-770.
23. L. J. Camras, K. E. Sufficool, C. B. Camras, S. Fan, H. Liu and C. B. Toris, *Curr Eye Res*, 2010, **35**, 819-827.
24. G. Li, P. Gonzalez, L. J. Camras, I. Navarro, J. Qiu, P. Challa and W. D. Stamer, *Experimental eye research*, 2013, **109**, 8-16.
25. C. L. P. Gonzalez, P. Challa, P. B. Liton, G. Li, J. Qiu, and D. L. Epstein, *Investigative ophthalmology & visual science*, 2008, **49**.
26. I. D. N. L.J. Camras, G. Li, J. Qiu, P. Challa, C. Luna, D.L. Epstein, P. Gonzalez, *Investigative ophthalmology & visual science*, 2010, **51**.
27. E. K. Dimitriadis, F. Horkay, J. Maresca, B. Kachar and R. S. Chadwick, *Biophysical journal*, 2002, **82**, 2798-2810.
28. D. C. Lin, E. K. Dimitriadis and F. Horkay, *Journal of biomechanical engineering*, 2007, **129**, 430-440.
29. M. Radmacher, *IEEE engineering in medicine and biology magazine : the quarterly magazine of the Engineering in Medicine & Biology Society*, 1997, **16**, 47-57.
30. H. Haga, S. Sasaki, K. Kawabata, E. Ito, T. Ushiki and T. Sambongi, *Ultramicroscopy*, 2000, **82**, 253-258.
31. C. T. McKee, J. A. Last, P. Russell and C. J. Murphy, *Tissue Eng Part B Rev*, **17**, 155-164.
32. J. A. Last, S. J. Liliensiek, P. F. Nealey and C. J. Murphy, *Journal of structural biology*, 2009, **167**, 19-24.
33. C. A. Grant, N. H. Thomson, M. D. Savage, H. W. Woon and D. Greig, *Journal of the mechanical behavior of biomedical materials*, 2011, **4**, 535-540.
34. D. Meller, K. Peters and K. Meller, *Cell and tissue research*, 1997, **288**, 111-118.
35. D. Zeng, T. Juzkiw, A. T. Read, D. W. Chan, M. R. Glucksberg, C. R. Ethier and M. Johnson, *Biomechanics and modeling in mechanobiology*, 2010, **9**, 19-33.
36. M. E. Dokukin, N. V. Guz and I. Sokolov, *Biophysical journal*, 2013, **104**, 2123-2131.
37. C. T. McKee, J. A. Last, P. Russell and C. J. Murphy, *Tissue Eng Part B Rev*, 2011, **17**, 155-164.
38. M. P. Wenger, L. Bozec, M. A. Horton and P. Mesquida, *Biophysical journal*, 2007, **93**, 1255-1263.

Figure legend

Figure 1. Rat anterior segment preparation for AFM analysis. (A) An enucleated rat eye was perfused with Evans blue solution, using a microneedle placed in the anterior chamber. (B) After perfusion, the eye was dissected, and the anterior segment was flat-mounted to a petri dish. The image shows the remnants of uveal tissue (black). (C) The image shows the TM stained with Evans blue. (D) The image shows the sclera in the anterior segment to be fixed to the petri dish surface for AFM analysis, using glass cover slips.

Figure 2. Rat anterior segment under an optical objective of AFM. (A) The image shows the five regions: (1) cornea, (2) corneal-TM, (3) TM, (4) TM-uveosclera, and (5) uveosclera. (B) The schematic shows how the five regions defined in Panel A are related to the locations of different tissues in a cross-section of anterior segment. The blue color indicates the distribution of Evens blue after whole eye perfusion.

Figure 3. Images of a histology section of the rat anterior segment. They were taken with A) a 40x objective and B) a 63x objective. The images confirmed the presence of the TM in the flat mounted anterior segment after dissection. Schlemm's canal (SC) is also clearly visible in the section.

Figure 4. A typical profile of force versus indentation. In experiments, we recorded the deflection of cantilever probe (d) and piezo-actuator translation (z), and used them to calculate the indentation (δ), the indentation force (F), and w. The contact point is at $w = w_c$, which is indicated by the triangle. The thin curve is the experimental data; and the thick curve is the regression curve, based on Equation 2. F_{max} was the value of F at the indentation of $0.5R$. Only the data between $F_{max}/3$ and F_{max} were used in curve fitting. For this specific data set, the regression analysis yielded: $(E_0)_{app}$ = 517 Pa, R^2 = 0.994, and w_c = 1.80 μm.

Figure 5. Images of AFM probe on top of a rat anterior segment. The tip of the probe was moved from Regions 1 through 5 to sequentially indent the tissues in an eye. The values of $(E_0)_{app}$ (Pa) determined for each region are also shown in the images. It could be observed that the minimum value of $(E_0)_{app}$ was reached in Region 3.

Figure 6. Box-and-whisker plots of experimental data for $(E_0)_{app}$. (A) The plot shows the results of $(E_0)_{app}$. The data for TM are also shown in the insert at a different scale. (B) The plot shows the results of $log_{10}E$, the logarithmically transformed $(E_0)_{app}$ with base 10, which appeared to be more symmetric about their medians.

Figure 7. A typical image of three-dimensional distribution of the total displacement in a rat anterior segment. It was generated through numerical simulations of the TM indentation. The level of total displacement is indicated by the color bar with the maximal value being equal to the indentation (δ). For this simulation, δ = R/2 where R is the AFM tip radius (i.e., 2.5 μm).

Figure 1

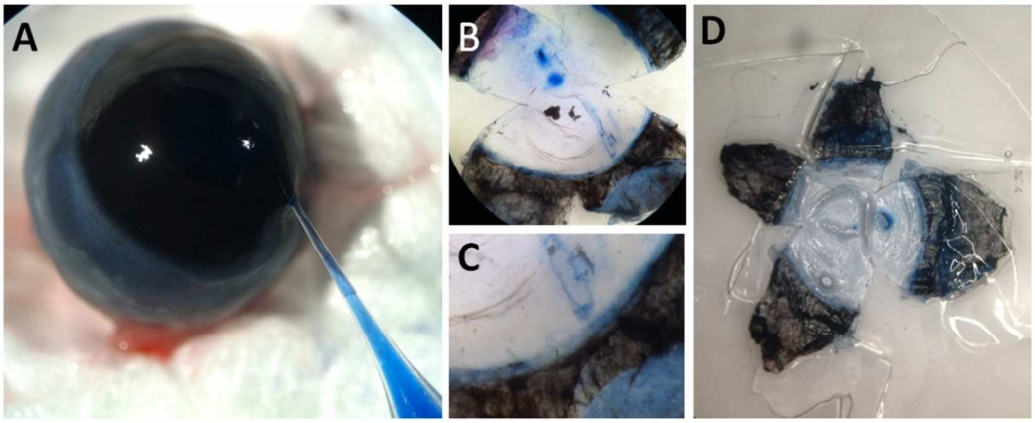

Figure 2

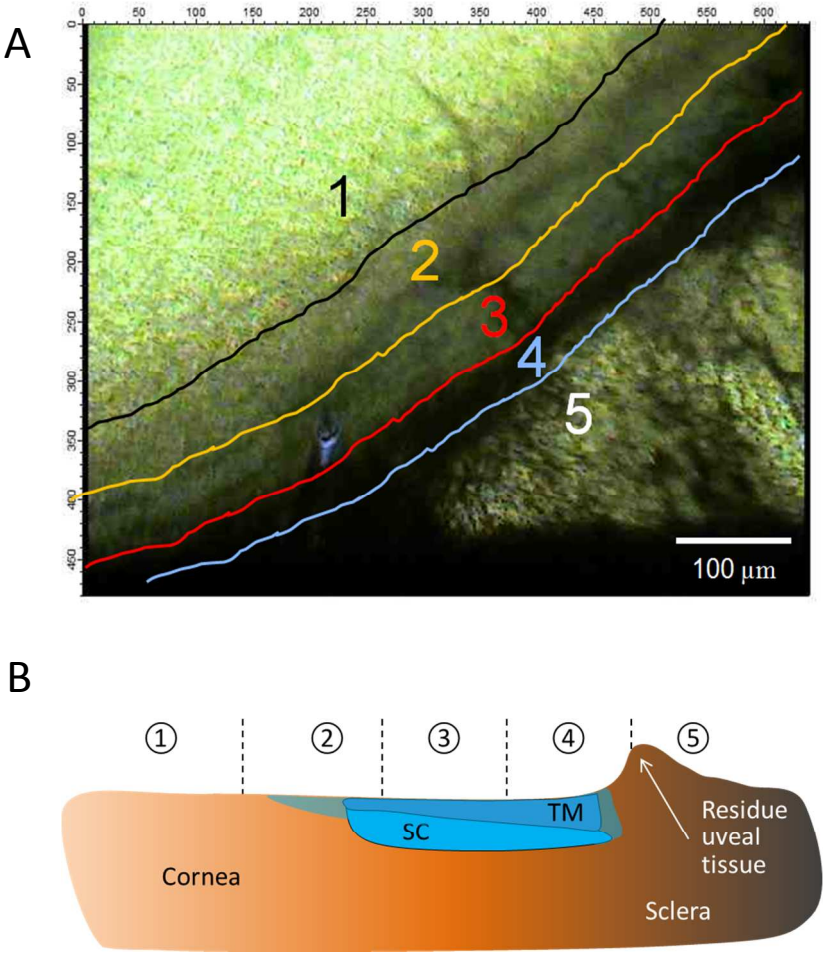
A
1
2
3
4
5
100 μm
B
①
②
③
④
⑤
TM
SC
Residue
uveal
tissue
Cornea
Sclera

Figure 3

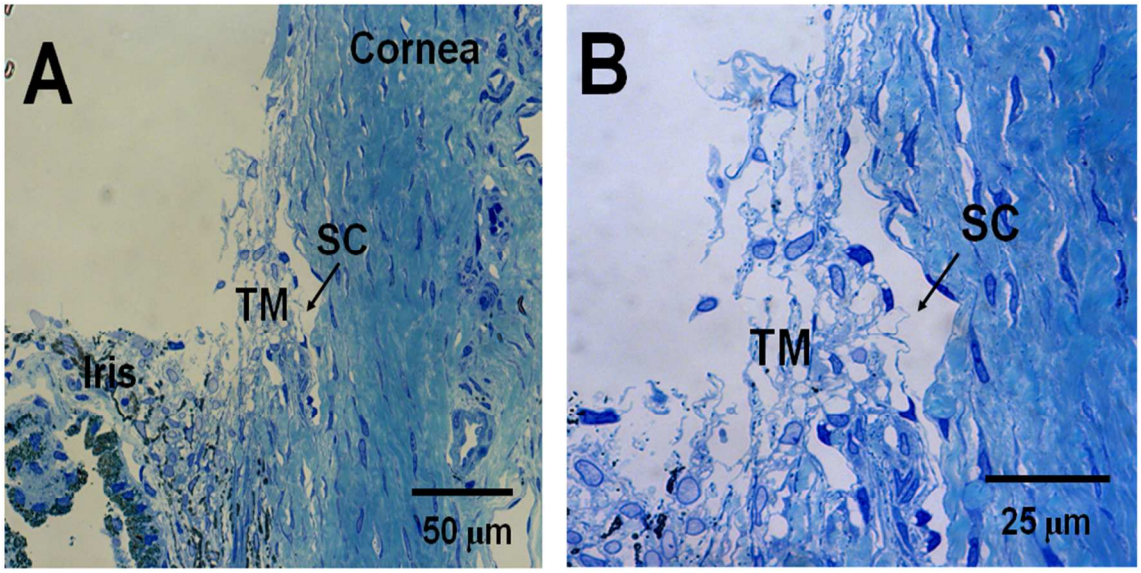

Figure 4

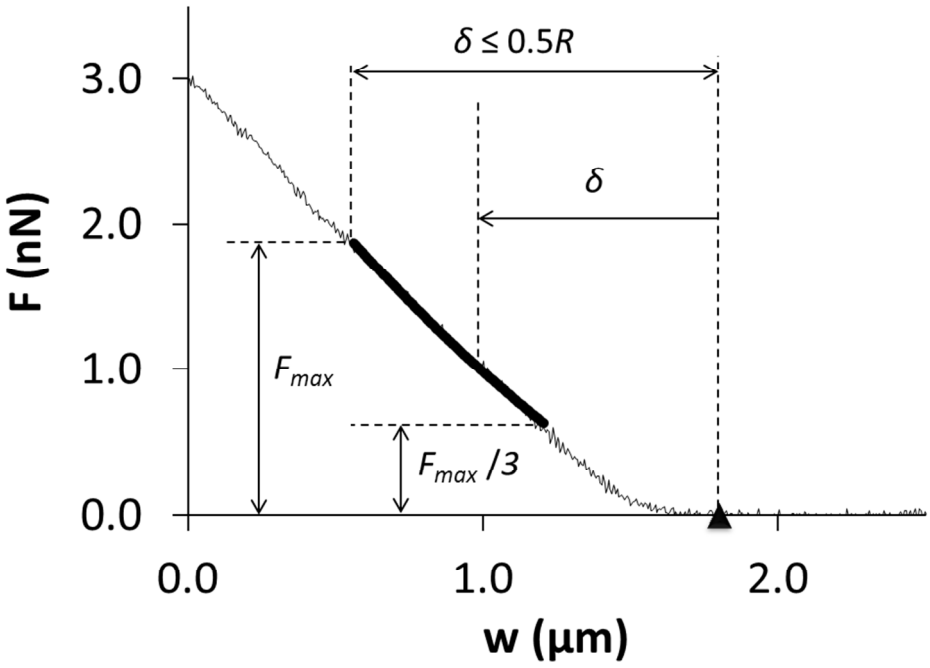

Figure 5

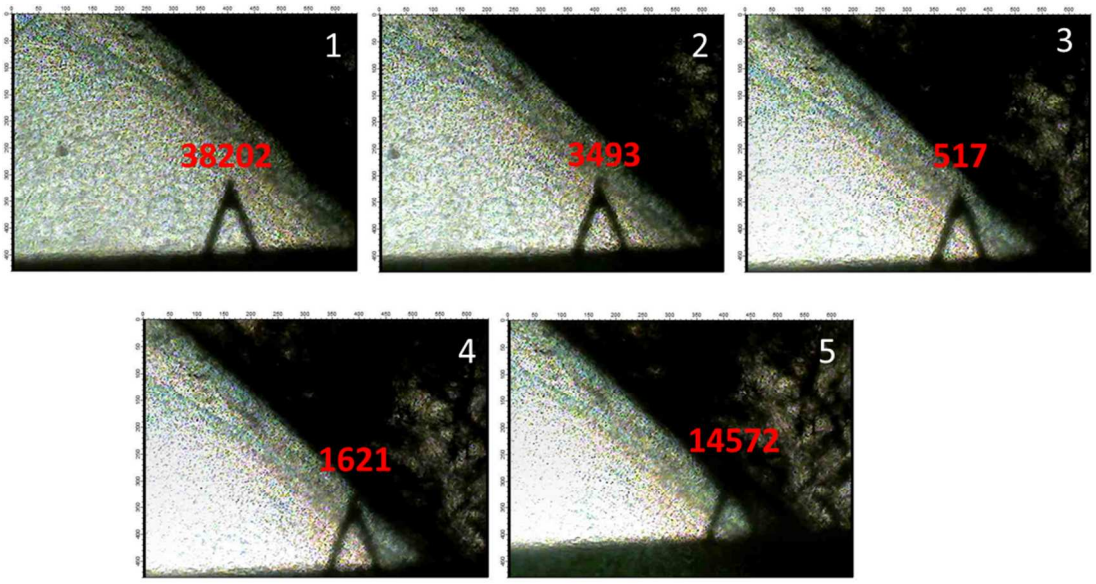

Figure 6

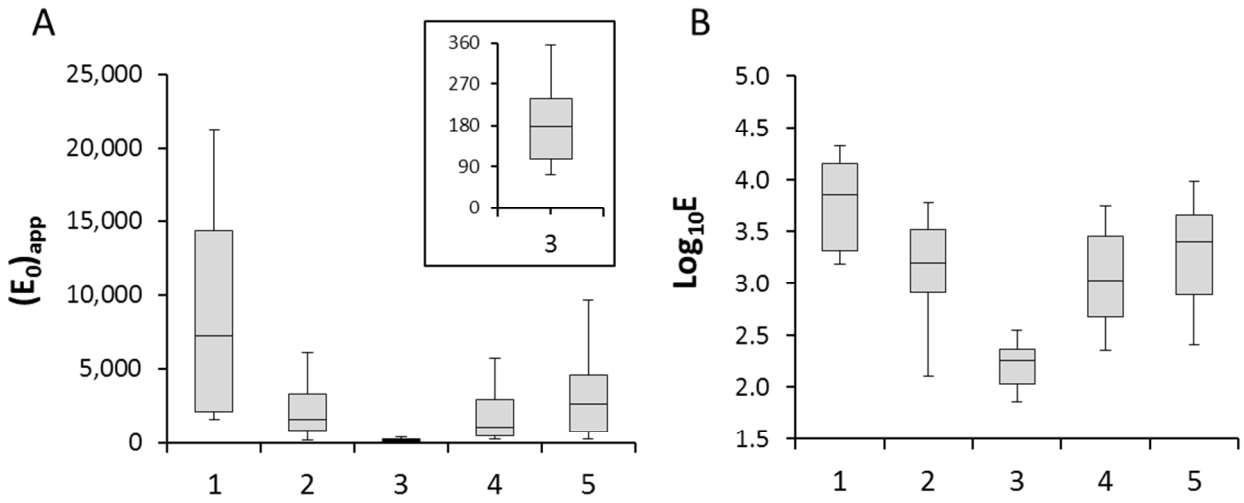
A
25,000
20,000
15,000
10,000
5,000
0
$(E_0)_{app}$
1
2
3
4
5
360
270
180
90
0
3
B
5.0
4.5
4.0
3.5
3.0
2.5
2.0
1.5
$Log_{10}E$
1
2
3
4
5

Figure 7

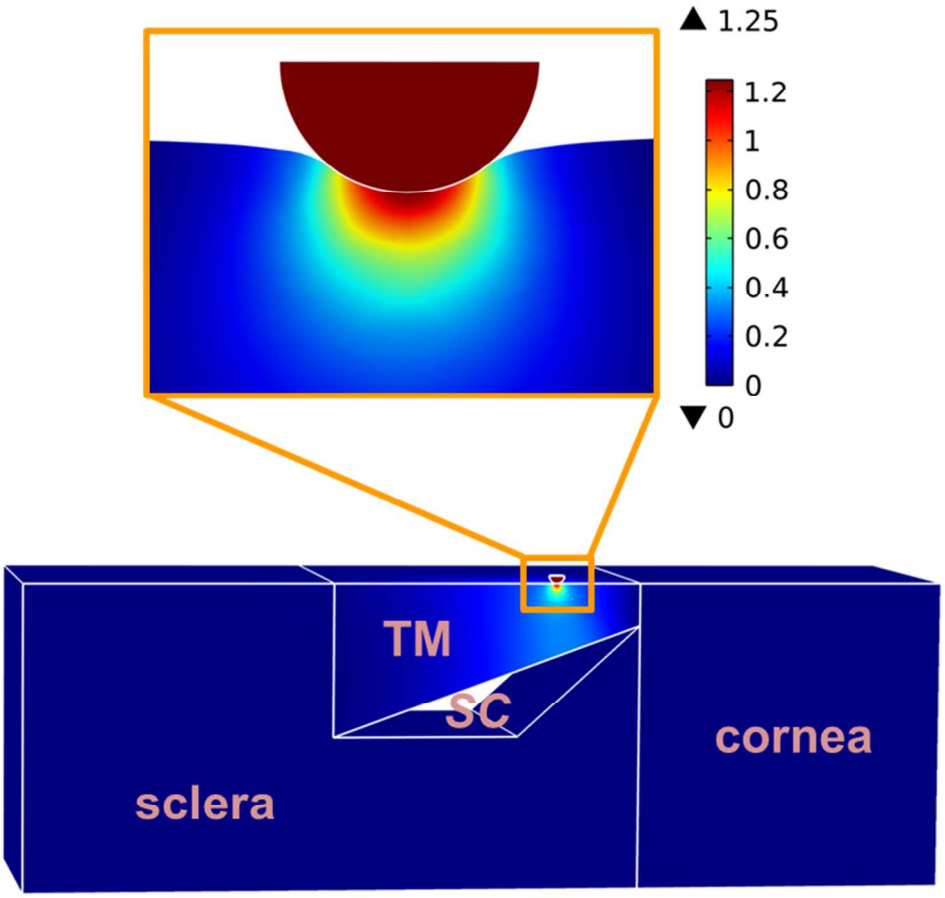

Graphic Table of Contents

We developed a method to quantify the initial Young's modulus of rat trabecular meshwork (TM) *in situ*, based on atomic force microscopy (AFM).